MATHEMATICAL MODELING METHODS FOR

A Post-Transcriptional Feedback Mechanism for Noise Suppression and Fate Stabilization

Maike M. K. Hansen[1]*, Winnie Y. Wen[1,2]*, Elena Ingerman[1]*, Brandon S. Razooky[1#,], Cassandra E. Thompson[1], Roy D. Dar[1&], Charles Chin[3], Michael L. Simpson[3], Leor S. Weinberger[1,4,5§]

[1]Gladstone Center for Cell Circuitry, Gladstone Institutes, San Francisco, CA 94158 United States; [2]Bioinformatics and Systems Biology Graduate Program, University of California, San Diego, La Jolla, CA 92093 United States; [3]Center for Nanophase Materials Science, Oak Ridge National Laboratory, Oak Ridge, TN 37831 United States; [4]Department of Pharmaceutical Chemistry and [5]Department of Biochemistry and Biophysics, University of California, San Francisco, CA 94158 United States

***** these authors contributed equally

[#] present address: Rockefeller University, New York City

[&] present address: University of Illinois, Urbana-Champaign

[§]Address for correspondence: leor.weinberger@gladstone.ucsf.edu

TABLE OF CONTENTS

Introduction and Rationale

We develop mathematical models of the HIV-1 full-length gene regulatory circuit to predict the overall architecture of HIV-1 gene-expression. The models are not intended to describe every biochemical step in HIV gene expression, but the goal is instead to find the minimal set of equations capable of fitting single-cell time-lapse imaging data. To achieve this, we compare and contrast the conventional HIV-1 co-transcriptional splicing mechanism to an HIV-1 post-transcriptional splicing cascade and also examine a 'mixed' model that includes both co-transcriptional and post-transcriptional splicing. Model fitting shows that post-transcriptional splicing is sufficient to fit the single-cell data. Parameter sensitivity analysis of the model is performed, and the model is validated by experimentally testing a non-intuitive prediction.

Construction of Mathematical Models of Full-Length HIV-1 Gene Regulation

We developed ordinary differential equation (ODE) models and simulated them using Berkeley Madonna™ and MATLAB™. General trend lines obtained from microscopic experiments were fit in Berkeley Madonna. Sensitivity analysis and parameter plots for the ODE model were performed in MATLAB or Berkeley Madonna. For stochastic simulations, chemical reaction schemes were coded in programming language C using the Gillespie algorithm (Gillespie, 2007; Gillespie et al., 2013). The simulation results were analyzed using MATLAB or Mathematica™.

We note that, in the interest of beginning with the simplest models and to reduce the number of fitting parameters during non-linear least-squares fitting, in the initial models (Eqs. 1–9), Tat positive feedback is assumed to saturate relatively early after infection, and thus, the Tat positive-feedback term is 'lumped' into the single Tat-independent basal rate parameter (b_{US}). This saturation assumption is subsequently relaxed in later models (Eqs. 10–13; "Experimental Validation of Model") where an explicit Tat positive-feedback term is added. Figure S5A shows that the single-cell time-lapse imaging data can be fit equally well by post-transcriptional splicing models assuming either active or saturated Tat positive feedback (while the fits are indistinguishable, certain parameter estimates do change).

Co-Transcriptional Splicing Model

We developed a set of five ODEs to describe the minimum full-length regulatory circuit of HIV-1 gene expression. To simplify the model, we assume the splicing of unspliced (US) RNA into singly spliced (SS) RNA is relatively fast compared to splicing of SS RNA to multiply-spliced (MS) RNA. Based on this simplifying assumption, one can lump unspliced and singly spliced RNA species and thereby limit explicit modeling to only two species of viral mRNA: unspliced (US) and multiply spliced (MS) RNA. To facilitate the future expansion and prediction of the models, we further classify US RNA into two classes based on the cellular localization. USn stands for the nuclear US RNA, and USc stands for the cytoplasmic US RNA. Because destabilized GFP (d2GFP) is used as the reporter throughout the experiments as a reporter in the *nef* reading frame,

we use d2GFP instead Nef in all of our models, and thus, the GFP level is representative of Nef levels. The nonlinear ODE system that describes the co-transcriptional splicing model is:

$$\frac{\mathrm{d}}{\mathrm{dt}}\mathrm{USn} = b_{US} - \frac{kr\cdot\mathrm{USn}\cdot\mathrm{Rev}^h}{{K_{Rev}}^h+\mathrm{Rev}^h} - drna\cdot\mathrm{USn} \quad (1)$$

$$\frac{\mathrm{d}}{\mathrm{dt}}\mathrm{USc} = \frac{kr\cdot\mathrm{USn}\cdot\mathrm{Rev}^h}{{K_{Rev}}^h+\mathrm{Rev}^h} - drna\cdot\mathrm{USc} \quad (2)$$

$$\frac{\mathrm{d}}{\mathrm{dt}}\mathrm{MS} = b_{MS} - drna\cdot\mathrm{MS} \quad (3)$$

$$\frac{\mathrm{d}}{\mathrm{dt}}\mathrm{Rev} = p\cdot fr\cdot\mathrm{MS} - dr\cdot\mathrm{Rev} \quad (4)$$

$$\frac{\mathrm{d}}{\mathrm{dt}}\mathrm{GFP} = p\cdot fg\cdot\mathrm{MS} - dg\cdot\mathrm{GFP} \quad (5)$$

where b_{US} is a lumped basal production rate consisting of US RNA transcription from the LTR promoter and Tat positive-feedback transactivation. *kr* is the maximum Rev-dependent RNA nuclear export rate, *h* is the Hill coefficient of the Rev-RRE interaction, K_{Rev} is the Michaelis-Menton saturation term for Rev nuclear export, *drna* is the RNA degradation rate, b_{MS} is the basal production rate of MS RNA directly from transcription and co-transcriptional splicing, *p* is the protein production rate per mRNA, *fr* is the fraction Rev-encoding RNA out of total MS RNA, *dr* is the degradation rate of Rev protein, *fg* is the fraction GFP-encoding RNA out of total MS RNA, and *dg* is the degradation rate of GFP protein. The rate parameters with literature estimates and justification are described in Table S2.

Eq. (1) describes three biochemical reactions: the basal production of USn, the Rev-dependent RNA nuclear export of USn, and the degradation of USn. In the rest of the system, there are only two reactions in each equation: production and degradation. Usc is produced solely from the Rev-dependent RNA nuclear export. For expediency, to simplify non-linear least-squares fitting, we first assume that Tat positive feedback saturates early in the system, and thus the Tat positive-feedback term is simplified into a single rate parameter and lumped with the basal transcription rate (this assumption is relaxed below in Eqs. 10–13 and Figure S5A shows that assuming either saturated or active, non-saturating Tat positive feedback does not change the ability of the equations to fit the data). The reactions of MS RNA nuclear export and Rev nuclear-cytoplasmic shuttling are much faster than other kinetic rates of the system and are thus not explicitly modeled.

Post-Transcriptional Splicing Model

The ODE systems for the post-transcriptional model is similar to the co-transcriptional model, but with two modified equations. First, Eq. (1), which describes USn dynamics in the co-transcriptional model, is replaced with the following equation:

$$\frac{\mathrm{d}}{\mathrm{dt}}\mathrm{USn} = b - sp\cdot\mathrm{USn} - \frac{kr\cdot\mathrm{USn}\cdot\mathrm{Rev}^{\mathrm{h}}}{{K_{Rev}}^{\mathrm{h}}+\mathrm{Rev}^{\mathrm{h}}} - drna\cdot\mathrm{USn} \quad (6)$$

where *b* is the lumped production rate of Tat-transactivated LTR transcription (i.e., basal plus Tat positive feedback), and *sp* is the rate of USn RNA spliced into MS RNA. Eq. (6) thus represents

four biochemical reactions: transcription, post-transcriptional splicing, Rev-dependent nuclear export, and degradation. Second, the Eq. (3) is modified as:

$$\frac{\mathrm{d}}{\mathrm{dt}}\mathrm{MS} = sp \cdot \mathrm{USn} - drna \cdot \mathrm{MS} \quad (7)$$

where MS RNA production is solely from the post-transcriptional splicing term in Eq (6). The other three housekeeping equations in this post-transcriptional model are the same as the equation (2), (4), and (5). Thus, the ODE system for post-transcriptional splicing is:

$$\frac{\mathrm{d}}{\mathrm{dt}}\mathrm{USn} = b - sp \cdot \mathrm{USn} - \frac{kr \cdot \mathrm{USn} \cdot \mathrm{Rev}^{\mathrm{h}}}{{K_{Rev}}^{\mathrm{h}} + \mathrm{Rev}^{\mathrm{h}}} - drna \cdot \mathrm{USn} \quad (6)$$

$$\frac{\mathrm{d}}{\mathrm{dt}}\mathrm{USc} = \frac{kr \cdot \mathrm{USn} \cdot \mathrm{Rev}^{h}}{{K_{Rev}}^{h} + \mathrm{Rev}^{h}} - drna \cdot \mathrm{USc} \quad (2)$$

$$\frac{\mathrm{d}}{\mathrm{dt}}\mathrm{MS} = sp \cdot \mathrm{USn} - drna \cdot \mathrm{MS} \quad (7)$$

$$\frac{\mathrm{d}}{\mathrm{dt}}\mathrm{Rev} = p \cdot fr \cdot \mathrm{MS} - dr \cdot \mathrm{Rev} \quad (4)$$

$$\frac{\mathrm{d}}{\mathrm{dt}}\mathrm{GFP} = p \cdot fg \cdot \mathrm{MS} - dg \cdot \mathrm{GFP} \quad (5)$$

"Mixed" Model (both co-transcriptional and post-transcriptional splicing)

To accommodate the possibility of both co-transcriptional and post-transcriptional splicing coexisting in HIV-1 mRNA processing, we also constructed a "mixed" model that included both processes. The purpose of the mixed model is to investigate if leakage from co-transcriptional splicing would disrupt the negative feedback resulting from the post-transcriptional splicing cascade. This system has five equations in total, two of which are modified from the other models:

$$\frac{\mathrm{d}}{\mathrm{dt}}\mathrm{USn} = b_{US} - sp \cdot \mathrm{USn} - \frac{kr \cdot \mathrm{USn} \cdot \mathrm{Rev}^{h}}{{K_{Rev}}^{h} + \mathrm{Rev}^{h}} - drna \cdot \mathrm{USn} \quad (8)$$

$$\frac{\mathrm{d}}{\mathrm{dt}}\mathrm{MS} = b_{MS} + sp \cdot \mathrm{USn} - \mathrm{drna} \cdot \mathrm{MS} \quad (9)$$

Eq. (8) is a mixture of Eq. (1) and (6), which consists of four biochemical events: the lumped co-transcriptional production of USn RNA, decay of USn due to post-transcriptional splicing, Rev-dependent nuclear export, and the RNA degradation. Eq. (9) is a chimeric version of Eq. (3) and (7), where MS RNA can be produced either from the co-transcriptional production or splicing from US RNA.

Model Selection by Nonlinear Least-Squares Regression of the ODE Models to Single-Cell Data

Single-cell time-lapse imaging data was fit to the above ODE systems using Berkeley Madonna™ (Figure 5B and S5A). Specifically, the general trend (i.e., mean trajectory) was fit by nonlinear least-squares fitting to the above three models using the parameter values summarized in Table S2. All initial conditions were set to zero to mimic viral infection or latent reactivation. To fit the single-cell data, the parameter estimates for *b*, *kr*, K_{Rev}, *h*, *fr*, and *fg* were allowed to vary, with the optimization parameter being the smallest possible Hill Coefficient, h. The parameter values used

for the post-transcriptional model after fitting are listed in the Table S2, and fit trajectories shown in Figure 5B and S5A. The fits indicate that only systems containing post-transcriptional splicing (the post-transcriptional model and the mixed model) produce the overshoot features shown in the data trajectory, with the post-transcriptional splicing model providing the best fit.

Parameter Sensitivity Analysis (Hill coefficient)

In many nonlinear ODE systems, the most sensitive parameters (i.e., those parameters that generate the most change in steady state values and pre-steady-state kinetics) are exponential multipliers, such as the Hill coefficients, that describe n^{th}-order self-cooperative reactions(Edelstein-Keshet, 1988). Here, we examine the model sensitivity to one such parameter: the cooperativity of Rev/RRE-dependent RNA nuclear export. HIV-1 Rev multimerizes and interacts with the RRE region in the intron-containing RNA. However, the exact number of bound Rev oligomers per RRE is unclear. Previous reports suggest that Rev binds to the RRE in ratios of either 2:1 (Daly et al., 1993), or 3:1 (Cook et al., 1991), or 4:1 (Daly et al., 1993; Mann et al., 1994; Pond et al., 2009), or 6:1 (Daugherty et al., 2010), or 8:1 (Cook et al., 1991; Daly et al., 1993), and even up to 12:1 (Mann et al., 1994). Here, we characterize the sensitivity of the post-transcriptional splicing model by fitting the model to the single-cell imaging data using different fixed (integer) values of the Hill coefficient *h* of Rev RNA nuclear export. Numerical simulations and least-squares fitting of the post-transcriptional splicing model indicate that the minimum value of *h* (the Hill coefficient of Rev/RRE-dependent RNA nuclear export) should be $h \geq 3$ to obtain a good fit ($R^2 \geq 0.9$) of the model to the single-cell imaging data (Figure S5B).

Experimental Validation of Model (Predictions)

To test if the resulting model made accurate predictions about viral expression, we set out to test a counter-intuitive prediction of the model: that over-expression of Rev (which is required for export of late viral transcripts (e.g., gag)) would *reduce* the level of late transcripts and their gene products. This counter-intuitive prediction arises because increased Rev exports late products too quickly, not allowing accumulation of sufficient Tat for positive feedback. Rev overexpression is simulated by modifying Eq. (4) to:

$$\frac{\mathrm{d}}{\mathrm{dt}}\mathrm{Rev} = b_{Rev} + p \cdot fr \cdot \mathrm{MS} - dr \cdot \mathrm{Rev} \qquad (10)$$

The extra parameter, b_{Rev}, is the production rate of Rev from an exogenous source other than HIV LTR. Experimentally, this can be performed by transfecting cells with Rev-encoding expression vectors. We overexpress Rev 24 hours before the onset of HIV-1 reactivation. Thus, the minimal Rev-only model will not be sufficient to describe the scenario, because the exogenous Rev will exist in the system before Tat positive feedback initiates HIV gene expression, in contrast to the previous minimal Rev negative-feedback model. As a result, the Tat positive feedback term in the ODE models cannot be simplified and lumped with the basal transcription in this case. Therefore, we replace Eq. (6) with the following:

$$\frac{\mathrm{d}}{\mathrm{dt}}\mathrm{USn} = b_{LTR} + \frac{\mathrm{kt}\cdot\mathrm{Tat}}{\mathrm{K_{Tat}}^{1} + q\cdot\mathrm{Tat}^{1}} - sp \cdot \mathrm{USn} - \frac{\mathrm{kr}\cdot\mathrm{USn}\cdot\mathrm{Rev}^{\mathrm{h}}}{\mathrm{K_{Rev}}^{\mathrm{h}} + \mathrm{Rev}^{\mathrm{h}}} - drna \cdot \mathrm{USn} \qquad (11)$$

where b_{LTR} is basal expression rate from LTR promoter, *kt* is the maximum Tat transactivation rate, and K_{Tat} is the Michaelis-Menten saturation concentration of Tat transactivation (for non-saturating positive feedback (Razooky et al., 2017), K_{Tat} is set to 0 and q set to 1). This new equation consists of the following elements: LTR basal transcription, Tat transactivation, post-transcriptional splicing, Rev-dependent nuclear export, and RNA degradation. We also add another equation to describe the Tat production and degradation:

$$\frac{\mathrm{d}}{\mathrm{dt}}\mathrm{Tat} = p \cdot ft \cdot \mathrm{MS} - dtat \cdot \mathrm{Tat} \qquad (12)$$

where *ft* is the fraction of Tat encoding MS RNA among all MS RNA, and *dtat* is the degradation rate of Tat protein. We begin by fitting the new Tat/Rev coupled feedback model to the single-cell imaging data (Figure 4 and 5, main text). The final parameters are listed in Table S2.

We simulated changes in expression dynamics upon Rev is overexpression. Initially, we assumed that the production of exogenous Rev reaches a steady state and calculate the initial Rev concentration from the following formula:

$$\mathrm{Rev}_{\mathrm{Initial}} = \frac{b_{Rev}}{dr} \qquad (13)$$

We used the model to predict the outcomes of exogenous Rev over expression. If viral gene expression is under Rev negative-feedback control, MS RNA production will be repressed, leading to lower Tat levels. Tat activates HIV-1 transcription by 20–60 fold (Bohan et al., 1992). Therefore, the effect of reduced viral expression due to Rev negative feedback would be amplified because of Tat transactivation. Accordingly, increased Rev negative feedback would lead to decreased levels of p24 and Nef.

We numerically probe the system by tuning b_{Rev}. Notably, when the b_{Rev} is not zero (i.e., Rev is overexpressed) GFP levels decrease (Figure S5C). Additionally, the model predicts that HIV-1 US RNA expression dynamics decrease (Figure S5D). Thus, the models suggested that Rev overexpression would lead to a decrease in the levels of both the MS and US gene products. We experimentally verified this prediction by transfecting Jurkat HIV-d_2G cells with an exogenous Rev expressing vector (Figure S5E and S5F).

Experimental Validation of Model (Wet-lab Testing)

Cell Line Nucleofector® Kit R (Lonza) was used to transfect pcRev plasmid DNA(Malim et al., 1988) into HIV-d2G Jurkat cells. For each transfection, 1.6×10^6 Jurkat cells and pre-set program O-028 were used. 10 ng/mL TNF-α was added into the culture 24 hours after transfection, and incubated for another 24 hours. Intracellular p24 was stained using anti-p24 antibody KC57-RD1 (Coulter Clone). Intracellular GFP and p24 levels were measured using flow cytometery (IntelliCyt™). Flow data were analyzed with FlowJo™ software. To verify the model's predictions, we transfected latently infected HIV-d_2G Jurkat cells with pcRev DNA (Malim et al., 1988), and activated the HIV-1 replication with TNF-α 24 hours post transfection. As predicted, increased Rev over-expression led to decreased levels of both GFP and p24, at 24 hours after activation (Figure S5E and S5F). Thus, the model successfully predicts and provides validation

for the overall model that serial post-transcriptional splicing and Rev nuclear export allow for negative-feedback regulation in HIV-1 gene expression.

Simplified Post-Transcriptional Splicing Model (Figure S3A)

To test if the observed MS mRNA maximum at ~60 minutes coincides with a maximum GFP expression at about 5–8 hours, we used a simplified version of the ODE post-transcriptional splicing model from above.

First, we simplified the Rev dependent export term in Eq. (6), to one lumped rate term *kex*:

$$\frac{\mathrm{d}}{\mathrm{dt}}\mathrm{USn} = b - sp \cdot \mathrm{USn} - kex \cdot \mathrm{Rev} \cdot \mathrm{USn} - drna \cdot \mathrm{USn} \quad (14)$$

$$\frac{\mathrm{d}}{\mathrm{dt}}\mathrm{USc} = kex \cdot \mathrm{Rev} \cdot \mathrm{USn} - drna \cdot \mathrm{USc} \quad (15)$$

Eq. (7) remained the same:

$$\frac{\mathrm{d}}{\mathrm{dt}}\mathrm{MS} = sp \cdot \mathrm{USn} - drna \cdot \mathrm{MS} \quad (7)$$

Rev and GFP production from Eqs. 4-5 were modified to include simplified lumped protein production rates *p*.

$$\frac{\mathrm{d}}{\mathrm{dt}}\mathrm{Rev} = p \cdot \mathrm{MSc} - dr \cdot \mathrm{Rev} \quad (16)$$

$$\frac{\mathrm{d}}{\mathrm{dt}}\mathrm{GFP} = p \cdot \mathrm{MSc} - dg \cdot \mathrm{GFP} \quad (17)$$

where, as above, *dr* is the degradation rate of Rev protein and *dg* is the degradation rate of GFP protein. Finally, we added a maturation step of GFP to fluorescent GFP (GFPmat):

$$\frac{\mathrm{d}}{\mathrm{dt}}\mathrm{GFPmat} = \mathrm{GFP} \cdot\ m - dg \cdot \mathrm{GFPmat} \quad (18)$$

where *m* is the maturation rate of GFP and *dg* is the degradation rate of GFP protein. See Table S2 for parameters used. Thus, the simplified ODE system for post-transcriptional splicing, including GFP maturation, is:

$$\frac{\mathrm{d}}{\mathrm{dt}}\mathrm{USn} = b - sp \cdot \mathrm{USn} - kex \cdot \mathrm{Rev} \cdot \mathrm{USn} - drna \cdot \mathrm{USn} \quad (14)$$

$$\frac{\mathrm{d}}{\mathrm{dt}}\mathrm{USc} = kex \cdot \mathrm{Rev} \cdot \mathrm{USn} - drna \cdot \mathrm{USc} \quad (15)$$

$$\frac{\mathrm{d}}{\mathrm{dt}}\mathrm{MS} = sp \cdot \mathrm{USn} - drna \cdot \mathrm{MS} \quad (7)$$

$$\frac{\mathrm{d}}{\mathrm{dt}}\mathrm{Rev} = p \cdot \mathrm{MSc} - dr \cdot \mathrm{Rev} \quad (16)$$

$$\frac{\mathrm{d}}{\mathrm{dt}}\mathrm{GFP} = p \cdot \mathrm{MSc} - dg \cdot \mathrm{GFP} \quad (17)$$

$$\frac{\mathrm{d}}{\mathrm{dt}}\mathrm{GFPmat} = \mathrm{GFP} \cdot\ \mathrm{m} - dg \cdot \mathrm{GFPmat} \quad (18)$$

Stochastic Simulations of Two-State Random Telegraph Model with Feedback

Stochastic simulations for Figure 2 were carried out on the Oak Ridge CNMS Beowulf cluster. Here, three models were compared.

The two-state (a.k.a. random telegraph) model consists of the following reaction scheme:

$$\mathrm{OFF} \xrightarrow{k_{on}} \mathrm{ON}$$
$$\mathrm{ON} \xrightarrow{k_{off}} \mathrm{OFF}$$
$$\mathrm{ON} \xrightarrow{\alpha} \mathrm{ON} + \mathrm{R}$$
$$\mathrm{R} \xrightarrow{\beta} \mathrm{R} + \mathrm{P}$$
$$\mathrm{R} \xrightarrow{\delta} \emptyset$$
$$\mathrm{P} \xrightarrow{\gamma} \emptyset$$

Where $k_{on} = 0.1$, $k_{off} = 1.0$, $\alpha = 20$, $\beta = 100$, $\delta = 1$, and $\gamma = 0.01$. As a benchmark, we examined reducing steady state twofold by setting $\alpha = 10$.

Negative feedback is introduced to reduce the steady state twofold using the following Transcriptional Auto-Repression model:

$$\mathrm{OFF} \xrightarrow{k_{on}} \mathrm{ON}$$
$$\mathrm{ON} \xrightarrow{k_{off}} \mathrm{OFF}$$
$$\mathrm{ON} \xrightarrow{\alpha} \mathrm{ON} + \mathrm{R}$$
$$\mathrm{R} \xrightarrow{\beta} \mathrm{R} + \mathrm{P}$$
$$\mathrm{R} \xrightarrow{\delta} \emptyset$$
$$\mathrm{P} \xrightarrow{\gamma} \emptyset$$
$$\mathrm{P} + \mathrm{OFF} \xrightarrow{\epsilon} \mathrm{Repressed}$$
$$\mathrm{Repressed} \xrightarrow{k_{unbind}} \mathrm{OFF} + \mathrm{P}$$

with all parameters as above and $\varepsilon = .001$ and $k_{unbind} = 8$ so that the steady state was reduced by half.

The Precursor Auto-Depletion feedback model uses the following reaction scheme:

$$\mathrm{OFF} \xrightarrow{k_{on}} \mathrm{ON}$$

$$\mathrm{ON} \xrightarrow{k_{off}} \mathrm{OFF}$$

$$\mathrm{ON} \xrightarrow{\alpha} \mathrm{ON} + pre$$

$$pre \xrightarrow{\theta} \mathrm{R}$$

$$\mathrm{P} + pre \xrightarrow{\epsilon} \mathrm{P} + 0$$

$$\mathrm{R} \xrightarrow{\beta} \mathrm{R} + \mathrm{P}$$

$$\mathrm{R} \xrightarrow{\delta} \emptyset$$

$$\mathrm{P} \xrightarrow{\gamma} \emptyset$$

with parameters as above and $\varepsilon = .0001$ and $\theta = 1$ so that the steady state was reduced by half.

As these parameter sets generate rather large numbers of simulated molecules, to mimic the physiological regimes (i.e., ~10^5 P molecules), desktop PCs were too slow and the simulations needed to be run on a cluster (ORNL CNMS cluster).

Transcriptional Auto-Repression Perversely *Increases* Noise, whereas Auto-Depletion Does Not

The following simulations were run in Mathematica™ using the xSSAlite™ on a PC.

As above, the two-state model is

$$\mathrm{OFF} \xrightarrow{k_{on}} \mathrm{ON}$$

$$\mathrm{ON} \xrightarrow{k_{off}} \mathrm{OFF}$$

$$\mathrm{ON} \xrightarrow{\alpha} \mathrm{ON} + \mathrm{R}$$

$$\mathrm{R} \xrightarrow{\beta} \mathrm{R} + \mathrm{P}$$

$$\mathrm{R} \xrightarrow{\delta} \emptyset$$

$$\mathrm{P} \xrightarrow{\gamma} \emptyset$$

with $k_{on} = 1.0$, $k_{off} = 0.001$, $\alpha = 20$, $\beta = 10$, $\delta = 1$, and $\gamma = 0.25$ it gives a steady-state value of P ≈ 800. In this parameter regime ($k_{on} >> k_{off}$), the model is essentially constitutive expression.

Negative feedback can be introduced to reduce the steady state twofold (i.e., P ≈ 400), using the following Transcriptional Auto-Repression model:

$$\mathrm{OFF} \xrightarrow{k_{on}} \mathrm{ON}$$

$$\mathrm{ON} \xrightarrow{k_{off}} \mathrm{OFF}$$

$$\mathrm{ON} \xrightarrow{\alpha} \mathrm{ON} + \mathrm{R}$$

$$\mathrm{R} \xrightarrow{\beta} \mathrm{R} + \mathrm{P}$$

$$\mathrm{R} \xrightarrow{\delta} \emptyset$$

$$\mathrm{P} \xrightarrow{\gamma} \emptyset$$

$$\mathrm{P} + \mathrm{ON} \xrightarrow{\epsilon} \mathrm{P} + \mathrm{OFF}$$

with parameters as above and $\varepsilon = .003$. This results in the steady state being reduced by half (i.e., $\mathrm{P} \approx 400$), compared to the unregulated two-state model.

As above, the Precursor Auto-Depletion feedback model uses the following reaction scheme:

$$\mathrm{OFF} \xrightarrow{\mathrm{k}_{on}} \mathrm{ON}$$

$$\mathrm{ON} \xrightarrow{\mathrm{k}_{off}} \mathrm{OFF}$$

$$\mathrm{ON} \xrightarrow{\alpha} \mathrm{ON} + pre$$

$$pre \xrightarrow{\theta} \mathrm{R}$$

$$\mathrm{P} + pre \xrightarrow{\epsilon} \mathrm{P} + 0$$

$$\mathrm{R} \xrightarrow{\beta} \mathrm{R} + \mathrm{P}$$

$$\mathrm{R} \xrightarrow{\delta} \emptyset$$

$$\mathrm{P} \xrightarrow{\gamma} \emptyset$$

with parameters as above and $\varepsilon = .03$ and $\theta = 10$, so that the steady state was reduced by half (i.e., $\mathrm{P} \approx 400$).

500 simulation runs were performed (in Mathematica™ using the xSSAlite™) for each model to calculate the mean and CV^2. The results of simulations of these models are shown in Figure S1B–C (mean ± standard deviation).

Here, the two-state model's mean-expression level $\langle \mathrm{P} \rangle$ is reduced twofold (e.g., from 800 proteins/cell to 400), the Fano increases from 8.5 to 9.5 (i.e., Poisson scaling). Under these parameters, increasing transcriptional auto-repression to reduce the mean by one-half actually increased noise (Fano = 30), an established result (Austin et al., 2006; Lestas et al., 2010; Swain, 2004). However, in this parameter regime, precursor auto-depletion reduced the mean by one-half and also reduced the noise (Fano = 5.6), despite the added noise source relative to transcriptional auto-repression (i.e., the extra species, *pre*). We also tested a simplified RNA-Depletion model (not shown in main text) that lacks an explicit precursor:

$$\mathrm{OFF} \xrightarrow{\mathrm{k}_{on}} \mathrm{ON}$$

$$\mathrm{ON} \xrightarrow{\mathrm{k}_{off}} \mathrm{OFF}$$

$$\mathrm{ON} \xrightarrow{\alpha} \mathrm{ON} + \mathrm{R}$$

$$\mathrm{P} + \mathrm{R} \xrightarrow{\epsilon} \mathrm{P} + 0$$

$$\mathrm{R} \xrightarrow{\beta} \mathrm{R} + \mathrm{P}$$

$$\mathrm{R} \xrightarrow{\delta} \emptyset$$

$$\mathrm{P} \xrightarrow{\gamma} \emptyset$$

with all parameters as above. For all models, initial conditions were always were set to zero for all state variables, except ON = 1. This model decreased the noise further to Fano = 3.2 (see Figure S1C).

For the precursor depletion and simple RNA depletion models, we explicitly included formation of a reversible [pre·P] complex or [P·R] complex, respectively:

$$\mathrm{P} + \mathrm{pre} \underset{k_r}{\overset{k_f}{\rightleftarrows}} [\mathrm{pre} \cdot \mathrm{P}] \xrightarrow{\epsilon} \mathrm{P} + 0$$

$$\mathrm{P} + \mathrm{R} \underset{k_r}{\overset{k_f}{\rightleftarrows}} [\mathrm{P} \cdot \mathrm{R}] \xrightarrow{\epsilon} \mathrm{P} + 0$$

These changes appeared to have little effect on the simulation results for either model.

Modeling Circuit-Relaxation Dynamics after a TNF Pulse-Chase Experiment (Figure 7)

In modeling for Figure 7 (main text), we first determined if a deterministic ODE model of post-transcriptional splicing (essentially, the model used for model validation above) could account for the relaxation dynamics of wild-type HIV and A7 mutants after a TNF exposure and removal experiment (i.e., pulse-chase experiment). The model used was a slight variation of the model used above for validation, specifically:

$$\frac{\mathrm{d}}{\mathrm{dt}}\mathrm{USn} = b_{LTR} + \mathrm{kt} \cdot \mathrm{Tat} - sp \cdot \mathrm{USn} - \frac{\mathrm{kr} \cdot \mathrm{USn} \cdot \mathrm{Rev}^{\mathrm{h}}}{\mathrm{K_{Rev}}^{\mathrm{h}} + \mathrm{Rev}^{\mathrm{h}}} - drna \cdot \mathrm{USn} \quad (11)$$

$$\frac{\mathrm{d}}{\mathrm{dt}}\mathrm{MS} = sp \cdot \mathrm{USn} - drna \cdot \mathrm{MS} \quad (7)$$

$$\frac{\mathrm{d}}{\mathrm{dt}}\mathrm{Tat} = p \cdot ft \cdot \mathrm{MS} - dtat \cdot \mathrm{Tat} \qquad (12)$$

$$\frac{\mathrm{d}}{\mathrm{dt}}\mathrm{Rev} = p \cdot fr \cdot \mathrm{MS} - dr \cdot \mathrm{Rev} \qquad (4)$$

$$\frac{\mathrm{d}}{\mathrm{dt}}\mathrm{GFP} = p \cdot fg \cdot \mathrm{MS} - dg \cdot \mathrm{GFP} \qquad (5)$$

with parameters as described in Table S2, except for the following modifications to account for the experiment performed: the splicing rate (*sp*) was increased by 10-fold (1.5 → 15) to model the A7 mutant (specifically, a 10-fold increase in *sp* corresponds to a ~2–3-fold increase in GFP steady state as seen in the A7 mutants; compare Figure 6, main text, to Figure S7). Changing *sp* was based on analysis (Figure 5C), showing that increasing the splicing rate, *sp*, is sufficient to abrogate the negative-feedback overshoot.

To simulate removal of TNF and cells relaxing to an OFF state, at time=48 h, b_{LTR} was instantaneously reduced by threefold [based on measurements from (Dar et al., 2012) and simultaneously *kt* was set to 0 to mimic the stochastic switching off of Tat, which formally requires stochastic models (Razooky et al., 2015; Weinberger et al., 2005). As shown Figure S7, this deterministic ODE model cannot fit the experimental relaxation dynamics after TNF removal. Specifically, the ODE model predicts that the A7 mutants will relax *slower* than wild-type HIV. The experimental data is the opposite (A7 mutants relax *faster* than wild-type HIV).

Given the inability of a deterministic model to fit the data, we then considered a stochastic version of the model. For simplicity and computational tractability, we first examined an RNA depletion model:

$$\mathrm{OFF} \xrightarrow{\mathrm{k}_{on}} \mathrm{ON}$$

$$\mathrm{ON} \xrightarrow{\mathrm{k}_{off}} \mathrm{OFF}$$

$$\mathrm{ON} \xrightarrow{\alpha} \mathrm{ON} + \mathrm{R}$$

$$\mathrm{P} + \mathrm{R} \underset{k_r}{\overset{k_f}{\rightleftarrows}} [\mathrm{P} \cdot \mathrm{R}] \xrightarrow{\epsilon} \mathrm{P} + 0$$

$$\mathrm{R} \xrightarrow{\beta} \mathrm{R} + \mathrm{P}$$

$$\mathrm{R} \xrightarrow{\delta} \emptyset$$

$$\mathrm{P} \xrightarrow{\gamma} \emptyset$$

using a 'pilot' set of parameters: with $k_{on} = k_{off} = 0.015$, $\alpha = 5$, $\beta = 10$, $\delta = 1$, $\gamma = 0.25$, $k_f = k_r = 0.5$, $\varepsilon = 0.015$. These parameter values were designated as "wild type". Initial conditions for all state variables OFF, R, P, P·R were set to zero except ON = 1. These parameter values were empirically chosen so that setting $k_f \rightarrow 0$, results in the steady-state P increasing by threefold as in the A7 mutant (main text Figure 6B). Simulations of the "mutant" were run with $k_f = 0$ and compared to

"wild-type" with parameters as above. For these pilot simulations, histograms were generated from 500 runs of each model at time = 100. The following plot shows representative simulation runs from this simulation (blue = wild-type HIV, orange = A7 mutant):

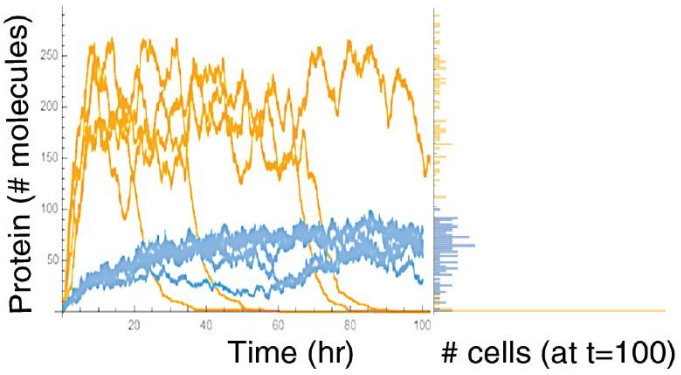

Given these promising simulation results, we then ran a more extensive simulation analysis using more physiological parameter estimates that generate molecular numbers of protein in the tens of thousands of molecules (Figure 7A and 7B, main text). The parameter values used for the simulations presented in Figure 7A and 7B (main text) are: $k_{on} = k_{off} = 0.015$, $\alpha = 500$, $\beta = 100$, $\delta = 1$, $\gamma = 0.25$, $k_f = 0.0002$ $k_r = 0.05$, $\varepsilon = 0.015$ (for the mutant, we set $k_f = k_r = \varepsilon = 0$). Initial conditions for all state variables OFF, R, P, P·R were set to zero except ON = 1. One thousand simulation runs of each wild-type and mutant parameter set were run, with each simulation run to time = 300. Given the computational intensity of these simulations (steady state P values were ~200,000 and ~50,000 molecules for each mutant and wild-type trajectory, respectively), the CNMS computing cluster at Oak Ridge National Laboratory was used for these simulations. Histograms of values of P at t = 300 were plotted in Mathematica™.

Analytic Arguments Supporting Precursor Auto-Depletion Minimization of Transcriptional Noise

Negative auto-regulation is accomplished by the repression of the average protein synthesis rate (k_p) by the protein. The strength of the feedback is described by a term known as the loop transmission (Simpson et al., 2003) where

$$T = \frac{\partial \mu}{\partial k_p}\frac{\partial k_p}{\partial \mu}$$

$$k_p = b_p \alpha O$$

$$O = \frac{k_{ON}}{(k_{ON} + k_{OFF})}$$

$$b_p = \frac{\beta}{\delta}$$

β and δ are as described above. The term b_p is often known as the translational burst size and is the average number of proteins synthesized using an individual mRNA template.

Negative feedback may operate by modulating any of the three terms that define k_p, and it has three main effects on gene circuit function: (1) reduction of the steady-state protein population (μ); (2) change of protein population noise and noise spectrum; (3) change in speed of responsiveness (i.e. bandwidth). Here we focus on only the first two effects, and find that the gene circuit noise with feedback is described by the relationships (Simpson et al., 2003)

$$Fano = \frac{Fano_{NFB}}{(1 + |T|)}$$

$$CV^2 = \frac{CV^2_{NFB}}{(1 + |T|)}$$

where the subscript NFB denotes a gene circuit where T=0 but is otherwise identical to the circuit with feedback (i.e., same steady-state populations and rates).

The noise in the protein population is often dominated by the noise introduced in the transcription process. Neglecting the feedback effect (i.e., assuming T=0), the power spectral density (PSD) of the noise in the protein population due to transcriptional noise ($S_{p-\alpha}(f)$) is (Cox et al., 2006)

$$S_{p-\alpha}(f) = S_\alpha(f) H^2_{\alpha-p}(f)$$

where $S_\alpha(f)$ is the PSD of noise in the rate of transcription and $H^2_{\alpha-p}(f)$ is the noise power gain between transcription and the protein population. Assuming that the protein decay time is the dominant time constant in the circuit (Simpson et al., 2003), the variance in the protein population (σ^2) is

$$\sigma^2 = \frac{\gamma}{4} S_\alpha(0) H^2_{\alpha-p}(0)$$

$$Fano = \frac{\sigma^2}{\mu} = \frac{\frac{\gamma}{4} S_\alpha(0) H^2_{\alpha-p}(0)}{\mu} = \frac{\frac{\gamma}{4} S_\alpha(0) H^2_{\alpha-p}(0)}{H_{\alpha-p}(0)\alpha O} = \frac{\gamma S_\alpha(0) H_{\alpha-p}(0)}{4\alpha O},$$

or

$$Fano = b_{r\_eff} b_{p\_eff}$$

where

$$b_{r\_eff} = \frac{S_\alpha(0)}{4\alpha O}$$

$$b_{p\_eff} = \gamma H_{\alpha-p}(0).$$

b_{r_eff} may be thought of as the *effective* burst size of transcription, and b_{p_eff} as the *effective* burst size of translation. Critically, transcriptional negative autoregulation modulates only b_{r_eff}, while precursor auto-depletion modulates only b_{p_eff}, and it is this difference that enables precursor auto-depletion to achieve superior noise performance as shown below.

From standard circuit analysis for the circuits described above, we find that for all transcriptional auto-repression circuits

$$b_{p\_eff} = b_p,$$

while for precursor auto-depletion,

$$b_{p\_eff} = b_p \left(\frac{\theta}{\theta + \epsilon}\right).$$

So *precursor auto-depletion always has a smaller effective translational burst size than all transcriptional auto-repression circuits*. To compare the transcriptional auto-repression and precursor auto-depletion, consider two-state transcriptional bursting where (Simpson et al., 2004)

$$S_\alpha(0) = 4\alpha O\left(1 + \frac{\alpha k_{OFF}}{(k_{ON} + k_{OFF})^2}\right)$$

$$b_{r\_eff} = 1 + \frac{\alpha k_{OFF}}{(k_{ON} + k_{OFF})^2}.$$

Considering a few cases provides some intuitive understanding of b_{r_eff}. For constitutive expression, $k_{OFF} \to 0$, and $b_{r\_eff} = 1$, and the simple interpretation is that each mRNA synthesis event is its own burst of a single mRNA molecule. Conversely, for the often-analyzed case of short, well-spaced transcriptional bursts (i.e. $k_{OFF} \gg k_{ON}$) then

$$b_{r\_eff} = 1 + \frac{\alpha}{k_{OFF}}$$

and the interpretation is that well-spaced bursts of mRNA are produced with an average burst size of $\frac{\alpha}{k_{OFF}}$. Between these extremes, the maximum b_{r_eff} occurs when $k_{OFF} = k_{ON}$ giving

$$b_{r\_eff\_max} = 1 + \frac{\alpha}{4k_{OFF}}.$$

Finally, in the limit where $k_{ON} \gg k_{OFF}$

$$b_{r\_eff} = 1 + \frac{\alpha k_{OFF}}{(k_{ON})^2} \approx 1,$$

and the interpretation is that the gene is in the ON state so often that expression is nearly constitutive. This final example is the state of the LTR promoter when the Tat protein level is high (i.e., just before the Rev-mediated negative feedback becomes activated). For this situation, the Fano factor of the protein level is completely determined by the effective translational burst size. Precursor auto-depletion acts to reduce the effective translational burst size, whereas auto-repression leaves the effective translational burst size unchanged from its maximum value of b_p. Furthermore, since auto-repression often operates by either decreasing k_{ON} or increasing k_{OFF}, it is even possible for this feedback to increase b_{r_eff} even up to its maximum possible value as was demonstrated in the simulations above. This produces the so-called "perverse effect" where negative feedback may lead to increased noise.

The table below summarizes the effects of auto-repression and precursor auto-depletion for various transcriptional motifs. The left-hand column describes expression before feedback is applied. Auto-repression operates by decreasing either α or k_{ON}, or by increasing k_{OFF}. Precursor auto-depletion operates by increasing ϵ. The right-hand comparison column assumes that both feedback motifs result in the same value of T.

Expression Motif (Without Feedback)	**Auto-Repression**	**Auto-Depletion**	**Comparison**
Two-state (k_{OFF}>>k_{ON})	$Fano = \frac{\left(1+\frac{\alpha}{k_{OFF}}\right)b_p}{1+\lvert T\rvert}$	$Fano = \frac{\left(1+\frac{\alpha}{k_{OFF}}\right)b_{p\_eff}}{1+\lvert T\rvert}$	Auto-depletion has lower noise but difference may be small if auto-repression operates by decreasing α or increasing k_{OFF}
Two-state (k_{ON}>>k_{OFF})	$\frac{b_p}{1+\lvert T\rvert} \le Fano \le \frac{b_{r\_eff\_max}b_p}{1+\lvert T\rvert}$	$Fano \approx \frac{b_{p\_eff}}{1+\lvert T\rvert}$	Auto-depletion has lower noise ($b_p > b_{p\_eff}$ and b_{r_eff} remains low). As shown in the simulation examples above, transcriptional auto-repression may lead to significantly higher noise.
Multistate	$Fano = \frac{b_{r\_eff}b_p}{1+\lvert T\rvert}$	$Fano = \frac{b_{r\_eff}b_{p\_eff}}{1+\lvert T\rvert}$	Auto-depletion has lower noise ($b_p > b_{p\_eff}$)

<u>Noise Suppression of Auto-Depletion Does Not Depend on a Two-State Model</u>

The analysis above demonstrates that precursor auto-depletion operates solely through manipulation of the apparent translational burst size. *As a result, the table above indicates the precursor auto-depletion effect is completely independent of the details of transcription, and it holds equally well for two-state (B_{eff}>1), or multistate (B_{eff}>1; see ref.(Corrigan et al., 2016)) expression.* The essential point is that since precursor auto-depletion operates by decreasing the effective translational burst size, it reduces noise for all transcriptional expression patterns where the noise of transcription dominates the noise behavior of the circuit.

Analytical Calculations Demonstrating that RNA Precursor Noise Is High Frequency

Without feedback, the core of the expression model with splicing is

$$\mathrm{ON} \xrightarrow{\alpha} \mathrm{ON} + pre$$

$$pre \xrightarrow{\theta} \mathrm{R}$$

$$pre \xrightarrow{\epsilon} \emptyset$$

$$\mathrm{R} \xrightarrow{\beta} \mathrm{R} + \mathrm{P}$$

$$\mathrm{R} \xrightarrow{\delta} \emptyset$$

$$\mathrm{P} \xrightarrow{\gamma} \emptyset$$

We define the following:

E_f = fraction of mRNA exported before splicing = $\frac{\epsilon}{\theta+\epsilon}$

Then, steady-state analysis yields:

Unspliced mRNA population: $\langle pre \rangle = \frac{\alpha}{\theta+\varepsilon}$

Spliced mRNA population: $\langle R \rangle = \frac{\alpha_{eff}}{\delta}$

Protein population: $\langle P \rangle = \frac{b_{eff}\alpha}{\gamma}$

Using the frequency domain formalism described in (Cox et al., 2006) (Equations 1-5), we first define the noise sources (note: since we assume b >> 1 we can neglect the noise source associated with translation).

There are four noise sources: (1) noise associated with transcription and discussed in detail previous sections, (2) noise associated with *pre* export, (3) noise associated with splicing *pre* into R, and (4) R decay. Noise terms (2) – (4) are white noise sources and, as described earlier, are often dominated by the bandlimited noise of transcription. However, splicing places an additional step in the mRNA decay process and will result in some additional noise.

In the frequency domain this gene circuit has three poles where:

$$f_1 = \frac{\varepsilon + \theta}{2\pi}$$

$$f_2 = \frac{\delta}{2\pi}$$

$$f_P = \frac{\gamma}{2\pi}$$

and the noise power gain for the splice noise is

$$H^2_{splice}(f) = \frac{b^2(E_f)^2}{(\gamma)^2}\left(\frac{1+\left(\frac{f}{E_f f_1}\right)^2}{\left(1+\left(\frac{f}{f_1}\right)^2\right)\left(1+\left(\frac{f}{f_2}\right)^2\right)\left(1+\left(\frac{f}{f_p}\right)^2\right)}\right).$$

Notably, this noise power gain includes a zero, indicating an increase in noise at higher frequencies. This high-frequency noise is the noise penalty of splicing and will be negligible as long as protein decay is slow compared to *pre* export or splicing rate. In summary, splice noise appears minimal and what noise it does add is high frequency and contributes little to the noise in protein levels as shown empirically in Figure S1C (compare CV of last two columns).

Detailed Explanation of Figure 2C i-iii

Analytical calculations of noise (Eqs. [1–2]) showing how precursor depletion (blue) surpasses the noise-suppression capabilities of transcriptional auto-repression (red). *T* is the same for both transcriptional auto-repression and precursor auto-depletion and *T=0* for the two-state model with no feedback (black). Solid lines were calculated from Eqs. [1–2] in the form $\frac{\sigma^2}{\mu^2} = \frac{b_R b_P}{\mu\cdot(1+|T|)}$. The numerical simulation results from panel B are superimposed on the analytical results as colored circles and can be explained using *Eq.* [1–2] as follows: (dotted arrow 'i') both transcriptional auto-repression and precursor auto-depletion reduce μ to half, but the former lowers μ by reducing f such that σ^2/μ^2 =γ/(f·(1+|T|)) remains at best constant (when feedback is maximal) whereas the latter lowers μ through reducing b_P, such that σ^2/μ^2 is decreased; (dotted arrow 'ii') once feedback saturates (T → 0), transcriptional auto-repression can continue to lower μ by further reducing f, which causes σ^2/μ^2 to increase corresponding to the perverse effect where auto-repression causes noise amplification (when kon >>koff, the two-state black line approaches constitutive expression and is closer to the origin and the red line and, hence, even for small decreases in μ, auto-repression perversely increases σ^2/μ^2). In contrast, since precursor auto-depletion lowers μ through reducing b_P, σ^2/μ^2 remains constant.